3-Dimensional Bond-based Peridynamic Representative Volume Element Homogenisation

Wenxuan Xia, Erkan Oterkus* and Selda Oterkus

PeriDynamics Research Centre, Department of Naval Architecture, Ocean and Marine Engineering

University of Strathclyde, Glasgow, UK

*Corresponding author: erkan.oterkus@strath.ac.uk

Abstract - In this study, a 3-Dimensional (3D) implementation of representative volume element homogenization using bond-based peridynamic formulation is presented. Periodic boundary condition is established by coupling the displacements of periodic point pairs. Homogenized (effective) material properties are obtained based on peridynamic displacement gradient tensor. The current approach is validated by considering a composite material without defects and comparing homogenized properties with results obtained from another homogenization approach. Next, the capability of the current approach is demonstrated by considering randomly generated cracks with arbitrary orientation and location. It can be concluded that the current approach can be an alternative approach to obtain 3-Dimensional homogenized material properties for heterogeneous materials with defects.

Keywords: peridynamics, homogenization, periodic boundary condition, bond-based, 3D

1. INTRODUCTION

To perform structural analysis at macroscopic scale, homogenized properties are utilized to approximately represent the material behavior. Although this approach usually gives reasonably accurate results, microstructural effects due to voids and micro-cracks can have significant influence on the macroscopic material behavior, especially fracture characteristics. Moreover, recently introduced micro-structured materials as a result of advances in 3-D printing and similar technologies require the consideration of the microstructural effects even further. To treat each individual microstructural effect as part of the analysis is usually intractable and homogenization approach is necessary which can also consider the effect of voids and micro-cracks.

There are various homogenization approaches available in the literature including rules of mixtures [1]. Homogenization process is usually done by performing volume averaging. Reuss and Voigt approaches provide the lower and upper limits of homogenized (effective) material properties [16]. In addition, a combination of finite element based representative volume element (RVE) has been developed. Moreover, asymptotic homogenization theory was introduced which is based on a two-scale formulation [20]. Although these approaches are effective for homogenization purposes, they can encounter difficulties to deal

with defects which cause discontinuities in the formulation. Spatial derivatives used as part of these homogenization approaches are not defined along crack surfaces. In such cases, finite element analysis can be a suitable option. However, special elements should be introduced to define the singularity at the crack tip [3]. Moreover, suitable crack propagation criteria should be introduced. Worth to mention that asymptotic homogenization, when used in combination with phase field approach, could potentially yield higher order parameters when properly applied. As an alternative, newly developed peridynamic formulation [4] can be more suitable since equations of motion of peridynamics are in the form of integro-differential equations and do not contain any spatial derivatives. Definition of failure is also pretty straightforward with respect to the ones used in traditional approaches. Peridynamics is suitable to analyze both isotropic, anisotropic [5] and polycrystalline [6] materials. It is possible to perform both static and dynamic fracture analysis [7]. Any number of cracks can occur in the material and it is possible to investigate the interaction of micro-cracks and macro-cracks [8][19]. Various peridynamic beam, plate and shell formulations are also available in the literature [9-11]. Homogenization can also be done within peridynamic framework [12]. In addition to structural analysis, peridynamics can also be used for the analysis of other physical fields [13-15].

As an extension of our earlier two-dimensional studies, in this study, peridynamic representative volume element homogenization approach is extended to three-dimensional configurations within bond-based peridynamic framework. Therefore, it will be possible to perform homogenization by considered defects such as microstructure.

To validate the current approach, peridynamic homogenization is performed by considering a composite material and effected properties are calculated. Peridynamic results are compared against another homogenization approach. Finally, to demonstrate the capability of the current approach, randomly oriented cracks are introduced in representative volume element to investigate their influence on effective material properties.

2. METHODOLOGY

2.1 BOND-BASED PERIDYNAMIC FORMULATION

Peridynamics was introduced by Silling [4] by reformulating the equations of continuum mechanics. For the original formulation, named as bond-based peridynamics, the equations of motion of the material point $\mathbf{x}$ can be expressed as [5]

$$\rho(\mathbf{x})\ddot{\mathbf{u}}(\mathbf{x},t)=\int_{H_{\mathbf{x}}}\mathbf{f}\left(\mathbf{u}'-\mathbf{u},\mathbf{x}'-\mathbf{x},t\right)dV'+\mathbf{b}(\mathbf{x},t) \quad (1)$$

In Eq. (1), H_k defines the domain of influence which is called as horizon. Therefore, material point $\mathbf{x}$ can interact with all material points $\mathbf{x}'$ inside its horizon with a size of δ. Note that peridynamic equations reduce to classical continuum mechanics equations as the horizon size converges to zero. $\mathbf{u}$ and $\mathbf{u}'$ are displacements of material points $\mathbf{x}$ and $\mathbf{x}'$, respectively. ρ, $\ddot{\mathbf{u}}$, $\mathbf{f}$ and $\mathbf{b}$ represent density, acceleration,

peridynamic force between two material points and body force, respectively.

It is usually not feasible to obtain analytical solution of the peridynamic equation given in Eq. (1). Therefore, numerical methods can be utilized based on meshless approach and Eq. (1) can be written in the discretized form as [5]

$$\rho(\mathbf{x}_k)\ddot{\mathbf{u}}(\mathbf{x}_k,t)=\sum_{j=1}^{N}\mathbf{f}_{kj}\left(\mathbf{u}_j-\mathbf{u}_k,\mathbf{x}_j-\mathbf{x}_k,t\right)V_j+\mathbf{b}(\mathbf{x}_k,t) \quad (2)$$

In Eq. (2), N represents the total number of material points denoted as j inside the horizon of the material point k. V_j is the volume of the material point j (see Fig. 1). $\mathbf{f}_{kj}$ is the peridynamic force between material points k and j which is defined as

$$\mathbf{f}_{kj}=\mathbf{f}\left(\mathbf{u}_j-\mathbf{u}_k,\mathbf{x}_j-\mathbf{x}_k,t\right)=cs\left(\mathbf{u}_j-\mathbf{u}_k,\mathbf{x}_j-\mathbf{x}_k,t\right)\frac{\mathbf{y}_j-\mathbf{y}_k}{\left|\mathbf{y}_j-\mathbf{y}_k\right|} \quad (3)$$

According to both based peridynamics, peridynamic force that the material point k is acting on material point j and the peridynamic force that the material point j is acting on material point k are equal in magnitude and opposite in direction. Therefore, both the conservations of linear and angular momentum are automatically satisfied. Moreover, the peridynamic force is only dependent on the motion of interacting material points.

The material constant in bond based peridynamics, c is called bond constant and can be represented in terms of elastic modulus of the material, E, as

$$c=\frac{12E}{\pi\delta^4} \quad (4)$$

Note that in bond-based peridynamics, the value of Poisson's ratio is constrained to the value of $\nu=1/4$.

The stretch of a peridynamic interaction (bond), s is defined as

$$s\left(\mathbf{u}_j-\mathbf{u}_k,\mathbf{x}_j-\mathbf{x}_k,t\right)=\frac{\left|\mathbf{y}_j-\mathbf{y}_k\right|-\left|\mathbf{x}_j-\mathbf{x}_k\right|}{\left|\mathbf{x}_j-\mathbf{x}_k\right|} \quad (4)$$

where $\mathbf{y}_k$ and $\mathbf{y}_j$ are new positions of the material points $\mathbf{x}_k$ and $\mathbf{x}_j$, in the deformed configuration.

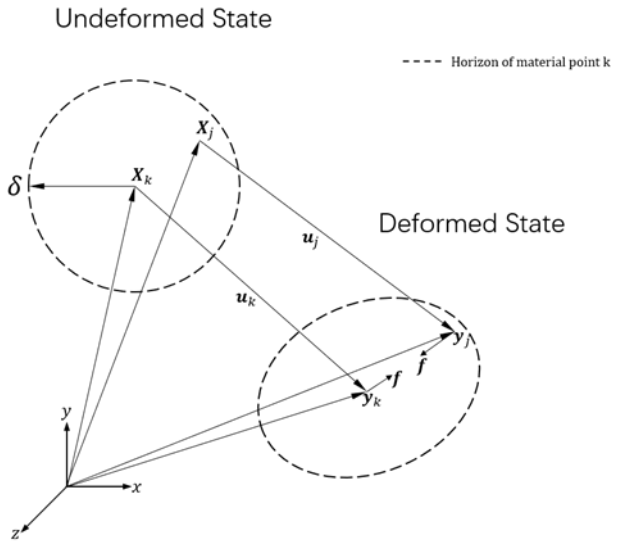

Fig.1. Definition of horizon and interaction between material points in bond-based peridynamic formulation.

In peridynamic formulation, since material points can interact with each other, interacting material points k and j can correspond to different materials. In such cases, the bond constant of the interaction between material points k and j can be obtained by splitting the interaction into multiple pieces (see Fig. 2a) and can be calculated as

$$c_{kj} = \psi_{kj}^{0} \frac{\sum_{m=1}^{M} d_m}{\sum_{m=1}^{M} \frac{d_m}{c^{(k,j;m)}}} \tag{6}$$

where M represents the number of pieces and d_m is the length of each piece of the interaction. For each piece, the bond constant $c^{(k,j;m)}$ can be calculated by using Eq. (4).

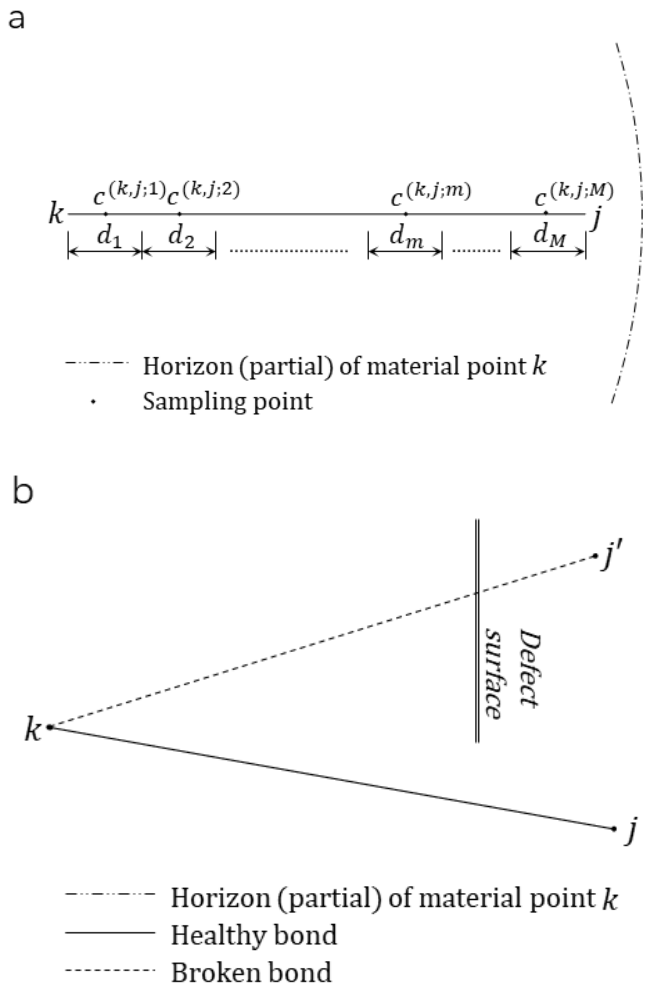

Fig. 2. (a) Pieces of a peridynamic interaction between material points k and j that correspond to different materials. **(b)** Healthy and broken bonds.

If an interaction is passing through a crack surface, then this bond will be broken (see Fig. 2b). To represent this, the parameter ψ_{kj}^{0} is introduced which is defined as

$$\psi_{kj}^{0} = \begin{cases} 0 & \text{if interaction passes through a crack surface} \\ 1 & \text{otherwise} \end{cases} \tag{7}$$

2.2 REPRESENTATIVE VOLUME ELEMENT FORMULATION

In this section, 3-Dimensional bond-based peridynamic representative volume element homogenization will be presented. To accomplish this, a representative volume element (RVE) will be defined to approximate the microscopic material properties of heterogeneous medium (microscale) as material properties of a statistically homogeneous medium (macroscale).

The macroscale will be denoted as (x) and the microscale will be denoted as (y). Only linear elastic deformations will be considered in this study. For a heterogeneous material at the microscale, the constitutive relationships can be expressed as [16]

$$\boldsymbol{\sigma} = \mathbf{C} \cdot \boldsymbol{\varepsilon} \tag{8a}$$

$$\boldsymbol{\varepsilon} = \mathbf{S} \cdot \boldsymbol{\sigma} \tag{8b}$$

where $\mathbf{S}$ and $\mathbf{C}$ represent compliance and stiffness tensors, respectively, and $\boldsymbol{\varepsilon}$ and $\boldsymbol{\sigma}$ represent microscopic strains and stresses, respectively.

Under the assumption of microstructure being periodic, a unit sized RVE can be utilized for the micromechanical analysis which corresponds to a material point in macroscale analysis. After the homogenization process, constitutive relationships can be represented at macroscale as [16]

$$\bar{\boldsymbol{\sigma}} = \mathbf{C}^{*} \cdot \bar{\boldsymbol{\varepsilon}} \tag{9a}$$

$$\bar{\boldsymbol{\varepsilon}} = \mathbf{S}^* \cdot \bar{\boldsymbol{\sigma}} \tag{9b}$$

where $\mathbf{S}^*$ and $\mathbf{C}^*$ represent homogenized (effective) compliance and stiffness tensors, respectively, and $\bar{\boldsymbol{\varepsilon}}$ and $\bar{\boldsymbol{\sigma}}$ represent macroscopic strains and stresses, respectively.

According to the homogenization theory, the macroscopic displacement $\bar{\mathbf{u}}$ can be expressed in terms of the microscopic displacement field $\mathbf{u}$ as [16]

$$\bar{\mathbf{u}} = \frac{1}{V}\int \mathbf{u}\, dV \tag{10}$$

where V is the volume of the RVE. Microscopic displacement field $\mathbf{u}$ calculated as

$$\mathbf{u} = \bar{\mathbf{u}} + \bar{\boldsymbol{\varepsilon}} \cdot x + \tilde{\mathbf{u}} \tag{11}$$

where $\bar{\mathbf{u}}$ is the volume averaged displacement, $\tilde{\mathbf{u}}$ is the displacement fluctuation function, and the average strain vector, $\bar{\boldsymbol{\varepsilon}}$, is defined as

$$\bar{\boldsymbol{\varepsilon}} = \frac{\partial \bar{\mathbf{u}}}{\partial x} \tag{12}$$

The macroscopic stress and strain can be expressed in terms of microscopic stresses and strains via volume averaging process as [16]

$$\bar{\boldsymbol{\sigma}} = \frac{1}{V}\int \boldsymbol{\sigma} dV \tag{13a}$$

$$\bar{\boldsymbol{\varepsilon}} = \frac{1}{V}\int \boldsymbol{\varepsilon} dV \tag{13b}$$

A constant strain tensor $\bar{\varepsilon}_{ij}$ is applied on a fictitious boundary region in peridynamic analysis and periodic boundary region relationship are expressed as shown in Fig. 3.

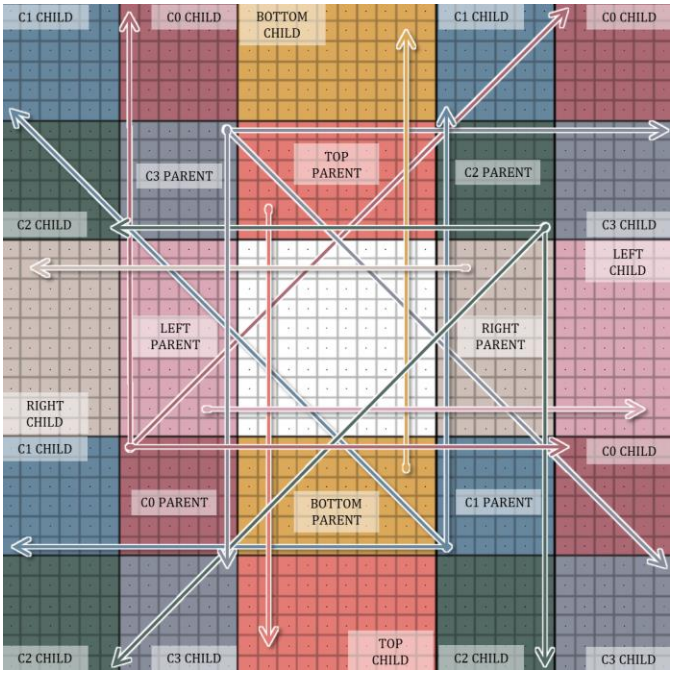

Fig. 3. Periodic boundary condition representation in peridynamic framework.

In Fig. 3, the outer fictitious regions are called as “Child”. The material points inside “Child” regions do not have their horizon. However, they can be considered as a material point within the horizon of non-fictitious material points. The regions next to “Child” regions are called “Parent” regions. Each material point inside a “Child” region is coupled with a material point inside a “Parent” region. On the other hand, each material point inside a “Parent” region can be linked to multiple material points in “Child” regions. The displacement of a material point inside a “Child” region depends on both the periodic condition and the displacement of the associated material point in “Parent” region. In contrast, the displacement of a material point in a “Parent” region depends on material points inside of its horizon regardless of these material points being inside the fictitious or non-fictitious regions.

In this study, the size of the fictitious region is considered as larger than twice of the horizon size so that all material points in the non-fictitious region has complete horizon and the periodic condition is satisfied.

The periodic relationship between material points inside "Child" and "Parent" regions can be expressed as

$$\mathbf{u}_i^c = \mathbf{u}_i^p + \bar{\boldsymbol{\varepsilon}}_{ij}\left(\mathbf{x}_j^c - \mathbf{x}_j^p\right) \tag{14}$$

where superscripts p and c denote paired material points inside "Parent" and "Child" regions respectively, (see Fig. 3), and $\bar{\boldsymbol{\varepsilon}}_{ij}$ is the macroscopic strain.

By using Eq. (11) and periodic boundary condition given in Eq. (14), the microscopic strain field $\boldsymbol{\varepsilon}$ can be obtained as

$$\boldsymbol{\varepsilon} = \bar{\boldsymbol{\varepsilon}} + \tilde{\boldsymbol{\varepsilon}} \tag{15}$$

If we substitute Eq. (13) into the constitutive relations given in Eq. (9), the relationship between microscopic stress and macroscopic strain can be obtained as

$$\mathbf{C}^*\bar{\boldsymbol{\varepsilon}} = \frac{1}{V}\int \boldsymbol{\sigma} dV \tag{16}$$

in which the macroscopic strain $\bar{\boldsymbol{\varepsilon}}$ is applied to the cell as boundary condition and can be defined as

$$\bar{\boldsymbol{\varepsilon}}_1^T = \left[c_s, 0, 0, 0, 0, 0\right] \tag{17a}$$

$$\bar{\boldsymbol{\varepsilon}}_2^T = \left[0, c_s, 0, 0, 0, 0\right] \tag{17b}$$

$$\bar{\boldsymbol{\varepsilon}}_3^T = \left[0, 0, c_s, 0, 0, 0\right] \tag{17c}$$

$$\bar{\boldsymbol{\varepsilon}}_4^T = \left[0, 0, 0, c_s/2, 0, 0\right] \tag{17d}$$

$$\bar{\boldsymbol{\varepsilon}}_5^T = \left[0, 0, 0, 0, c_s/2, 0\right] \tag{17e}$$

$$\bar{\boldsymbol{\varepsilon}}_6^T = \left[0, 0, 0, 0, 0, c_s/2\right] \tag{17f}$$

in which c_s is a small scalar value controlling the magnitude of the macroscopic strain.

The microscopic stress tensor $\boldsymbol{\sigma}$ can be obtained from the displacement-based homogenization result. As given in Breitenfeld et. al. [17], the peridynamic stress vector $\mathbf{s}$ at material point k can be obtained from displacement vector $\mathbf{U}$ as

$$\mathbf{s} = \left[\sigma_{11} \quad \sigma_{22} \quad \sigma_{33} \quad \sigma_{12} \quad \sigma_{13} \quad \sigma_{23}\right]^T = \mathbf{DKNU} \tag{18}$$

in which $\mathbf{D}$ is the isotropic elastic moduli matrix, $\mathbf{K}$ is the 3x3 shape tensor stored in a 6x9 matrix [17], and the definition for $\mathbf{N}$ is given in [17], which is a 9x3n matrix with n being the number of material points within k's horizon. The displacement vector $\mathbf{U}$ is assembled as [17]

$$\mathbf{U} = \left[u_k \quad v_k \quad w_k \quad \ldots \quad u_j \quad v_j \quad w_j \quad \ldots\right] \tag{22}$$

where u, v and w are the displacement components in x, y and z direction, respectively. Peridynamic stress tensor $\boldsymbol{\sigma}$ can then be assembled from peridynamic stress vectors $\mathbf{s}$ for every material point.

Finally, the effective stiffness tensor $\mathbf{C}^*$ can be assembled column by column from the peridynamic stress tensor $\boldsymbol{\sigma}$ and the macroscopic strain $\bar{\boldsymbol{\varepsilon}}$ as

$$\begin{Bmatrix} C_{1,i} \\ C_{2,i} \\ C_{3,i} \\ C_{4,i} \\ C_{5,i} \\ C_{6,i} \end{Bmatrix} = \begin{Bmatrix} \left\langle \sigma_i^{xx} \right\rangle \\ \left\langle \sigma_i^{yy} \right\rangle \\ \left\langle \sigma_i^{zz} \right\rangle \\ \left\langle \sigma_i^{yz} \right\rangle \\ \left\langle \sigma_i^{zx} \right\rangle \\ \left\langle \sigma_i^{xy} \right\rangle \end{Bmatrix} / c_s, \quad (i = 1, \ldots, 6) \tag{23}$$

where the angle bracket denotes the volume average over cell domain.

3. NUMERICAL RESULTS

The current approach is validated by considering a boron aluminum composite cell as shown in Fig. 4. The homogenized material properties from peridynamics are compared with the results from variational asymptotic method for unit cell homogenization (VAMUCH) [18]. The constituent properties for the boron aluminum composite are given in Table 1. In numerical analysis, a three-dimensional unit cell is considered with a discretization of 60x60x60. The spherical horizon size, δ is specified as 3 times of discretization size. Homogenized (effective) material properties are obtained by using Eqs. (16)-(23) and tabulated in Table 2. According to these results, a good agreement is achieved between results from peridynamic homogenization approach and VAMUCH approach.

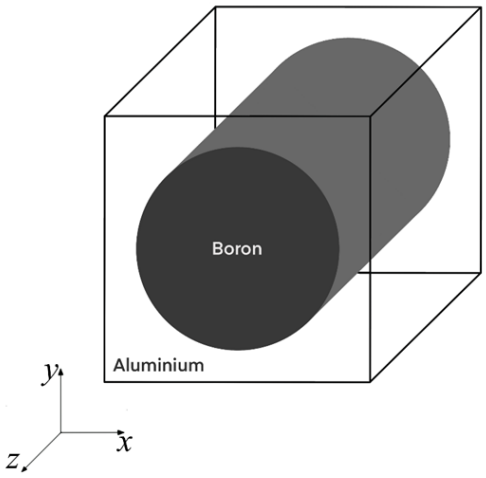

Fig. 4. Composite cell made of Boron aluminum.

Table 1. Constituent properties for boron and aluminum composite

Material name	Elastic modulus E (GPa)	Poisson's Ratio v	Volume fraction
Boron	379.3	0.25	0.47
Aluminum	68.3	0.25	0.53

The second example considers a three-dimensional aluminum cube contains arbitrarily oriented cracks as shown in Fig. 5. The material properties for aluminum used in this example are identical to the aluminum properties listed in Table 1.

Table 2. Homogenized properties of boron aluminum composite

	E_1 (GPa)	E_2 (GPa)	G_{12} (GPa)
Bond-based peridynamics	214.8	149.4	58.1
VAMUCH [18]	214.5	136.9	54.1

The cell geometry is considered to have unit dimension. The effective strength of such a cell is influenced by parameters such as crack orientation, crack density and crack shape etc. A pseudo crack density parameter is defined as

$$\rho = NA/V \tag{24}$$

where N is the total number of cracks, A is the surface area of an individual crack and V is the volume of the cell.

All cracks share the same dimension as shown in Fig. 6 where $w = 0.1m$ and $h = 0.05m$. However, the location and spatial orientation of each crack is

randomly generated. Rule is set so that no generated crack penetrates outside cell domain.

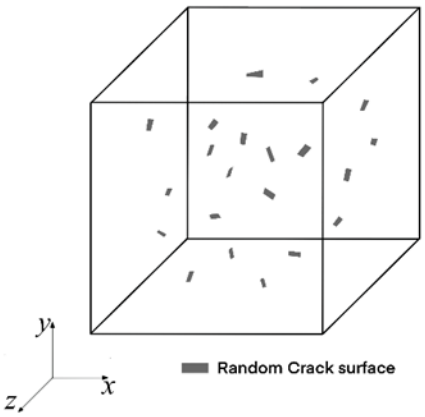

Fig. 5. Aluminum cell with random cracks.

Each crack has two unique properties: a location vector $\mathbf{x}(x,y,z)$ pointing towards the center of the crack, and a spatial rotation revolving around the crack center denoted as quaternion $\mathbf{q}(a,b,c,w)$. The purpose of representing crack rotation in a quaternion form is to accurately and conveniently obtain the Cartesian coordinates of four crack corner points. Although common Euler rotation can be applied, it tends to suffer from issues such as Gimbal lock and accuracy loss. Unit quaternions on the other hand does not have those limitations. The location vector can be simply generated using a random number generator. However, in order to generate randomly distributed quaternions in a uniform way, a hypersphere in four-dimensional space called Hopf fibration is created and chosen as selection space for quaternions. Once randomly generated vector $\mathbf{x}$ and quaternion $\mathbf{q}$ are applied to the crack, the Cartesian coordinates of corner points $c0$, $c1$, $c2$ and $c3$ are calculated.

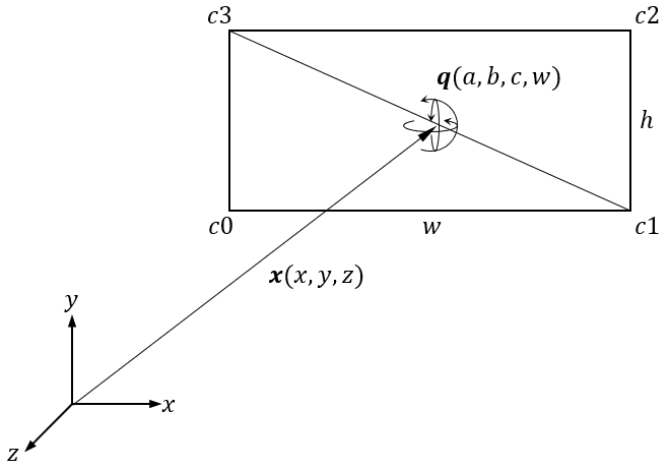

Fig. 6. Random three-dimensional crack location and orientation.

Crack is numerically represented by simply breaking peridynamic bonds as shown in Fig. 2b. To determine which bond meets the breaking criteria require intersection check between bond and cracks. In this study, two separate ray casting tests are performed for each pair of bond/crack candidate to determine if the bond intersects with a given crack. The crack as shown in Fig. 6 is divided into two triangles, triangle $c0-c1-c3$ and $c1-c2-c3$. One ray casting test is performed for each triangle.

Six crack densities are considered in this example: ρ = 0.1, 0.2, 0.3, 0.4, 0.5 and 0.6. Crack amount N is rounded into its nearest integer if necessary. Five instances are generated for each crack density level to obtain average results for comparison. List of crack densities and their corresponding crack amount is shown in Table. 3.

Table 3. Randomly generated cracks under different crack densities

Crack density ρ	0.1	0.2	0.3	0.4	0.5	0.6
Crack amount N	20	40	60	80	100	120

A total of 30 numerical cases are performed. Examples are solved with 20x20x20 peridynamic discretization. Spherical horizon with δ equivalent to 3 times of discretization size is chosen.

Numerical results are shown in Fig. 7 and Fig. 8 where E_x, E_y and E_z are reduced effective elastic moduli in *x*, *y* and *z* directions, respectively. The reduction in elastic modulus is resulted from the influence of cracks presented within the cell. The impact is measured by comparing the reduced modulus E_x, E_y and E_z against their original undamaged counterpart E_x^0, E_y^0 and E_z^0. The ratio E/E^0 is denoted as an elastic softening parameter ψ_E. Similarly, G_{xy}, G_{yz} and G_{xz} are reduced effective shear modulus. Material softening parameter ψ_G is defined as G/G^0, where G^0 is undamaged shear modulus.

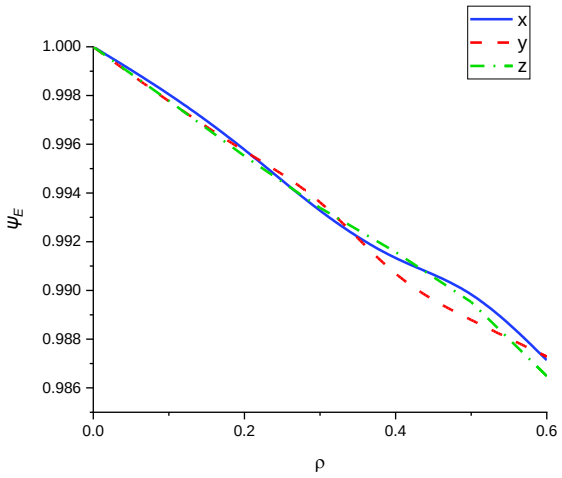

Fig. 7. Effective elastic modulus

When material softening happens due to the presence of cracks, parameter ψ_E and ψ_G will reduce accordingly.

For the randomly generated arbitrary oriented microcracks, the effective material properties in each direction decrease at the same rate while the crack density increases.

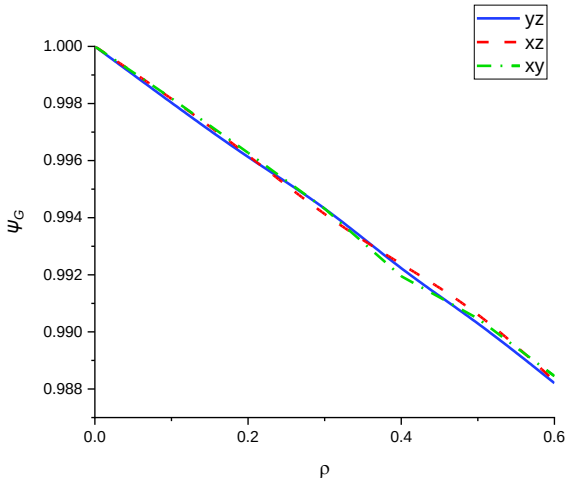

Fig. 8. Effective shear modulus

4. CONCLUSIONS

In this study, a 3-dimensional bond-based peridynamic representative volume element

homogenization method for heterogeneous materials with defects is presented. The current approach is verified by considering a boron-aluminum composite cell and comparing homogenized material results with results obtained from another homogenization method. The homogenization of a unit cell with randomly generated arbitrarily orientated micro-cracks with different crack densities is also performed. It is observed that by increasing crack density, effective stiffness reduces at the same rate in both x, y and z directions. Therefore, it can be concluded that the current approach can be a suitable alternative for homogenization of heterogeneous materials with defects. Future study can be done to improve current method with ordinary state-based PD formulation, which will provide more homogenization options in terms of material properties such as Poisson's ratio.

ACKNOWLEDGEMENT

The authors would like to dedicate this study to Prof. Siegfried Schmauder for his 65th birthday.

REFERENCES

1. Swan, C.C. and Kosaka, I., Voigt–Reuss topology optimization for structures with linear elastic material behaviours, *International Journal for Numerical Methods in Engineering*, 1997, vol. 40, no.16, pp. 3033-3057.

2. Fish, J., Shek, K., Pandheeradi, M. and Shephard, M.S., Computational plasticity for composite structures based on mathematical homogenization: Theory and practice, *Computer Methods in Applied Mechanics and Engineering*, 1997, vol. 148, no. 1-2, pp. 53-73.

3. Zi, G. and Belytschko, T., New crack-tip elements for XFEM and applications to cohesive cracks, *International Journal for Numerical Methods in Engineering*, 2003, vol. 57, no. 15, pp. 2221-2240.

4. Silling, S.A., Reformulation of elasticity theory for discontinuities and long-range forces, *Journal of the Mechanics and Physics of Solids*, 2000, vol. 48, no. 1, pp. 175–209.

5. Madenci, E. and Oterkus, E., *Peridynamic Theory and Its Applications*, New York, NY: Springer, 2014.

6. Zhu, N., De Meo, D. and Oterkus, E., Modelling of granular fracture in polycrystalline materials using ordinary state-based peridynamics, *Materials*, 2016, vol. 9, no. 12, p. 977.

7. Imachi, M., Tanaka, S., Ozdemir, M., Bui, T.Q., Oterkus, S. and Oterkus, E., Dynamic crack arrest analysis by ordinary state-based peridynamics, *International Journal of Fracture* 2020, vol. 221, no. 2, pp. 155–169.

8. Basoglu, M.F., Zerin, Z., Kefal, A. and Oterkus, E., A computational model of peridynamic theory for deflecting behavior of crack propagation with micro-cracks, *Computational Materials Science*, 2019, vol. 162, pp. 33–46.

9. Nguyen, C.T. and Oterkus, S., Peridynamics formulation for beam structures to predict damage in offshore structures, *Ocean Engineering*, 2019, vol. 173, pp.244-267.

10. Yang, Z., Vazic, B., Diyaroglu, C., Oterkus, E. and Oterkus, S., A Kirchhoff plate formulation in a state-based peridynamic framework, *Mathematics*

and Mechanics of Solids, 2020, vol. 25, no. 3, pp. 727–738.

11. Nguyen, C.T. and Oterkus, S., Peridynamics for the thermomechanical behavior of shell structures, *Engineering Fracture Mechanics*, 2019, vol. 219, p. 106623.

12. Madenci, E., Barut, A. and Phan, N., Peridynamic unit cell homogenization for thermoelastic properties of heterogenous microstructures with defects, *Composite Structures*, 2018, vol. 188, pp. 104–115.

13. De Meo, D. and Oterkus, E., Finite element implementation of a peridynamic pitting corrosion damage model, *Ocean Engineering*, 2017, vol. 135, pp. 76–83.

14. Diyaroglu, C., Oterkus, S., Oterkus, E. and Madenci, E., Peridynamic modeling of diffusion by using finite-element analysis, *IEEE Transactions on Components, Packaging and Manufacturing Technology*, 2017, vol. 7, no. 11, pp. 1823–1831.

15. Diyaroglu, C., Oterkus, S., Oterkus, E., Madenci, E., Han, S. and Hwang, Y., Peridynamic wetness approach for moisture concentration analysis in electronic packages, *Microelectronics Reliability*, 2017, vol. 70, pp. 103–111.

16. Cioranescu, D. and Donato, P., *An Introduction to Homogenization* (Vol. 17). Oxford: Oxford University Press, 1999.

17. Breitenfeld, M.S., Geubelle, P.H., Weckner, O. and Silling, S.A., Non-ordinary state-based peridynamic analysis of stationary crack problems, *Computer Methods in Applied Mechanics and Engineering*, 2014, vol. 272, pp. 233-250.

18. Yu, W. and Tang, T., Variational asymptotic method for unit cell homogenization of periodically heterogeneous materials, *International Journal of Solids and Structures*, 2007, vol. 44, no. 11-12, pp. 3738-3755.

19. Candaş, A., Oterkus, E., İmrak, C.E., Dynamic crack propagation and its interaction with micro-cracks in an impact problem, *Journal of Engineering Materials and Technology*, Transactions of *ASME*, 2021, vol. 143(1): 011003.

20. Kalamkarov, A.L., Andrianov, I.V. and Danishevs'kyy, V.V., Asymptotic homogenization of composite materials and structures, *Applied Mechanics Reviews*, 2009, vol. 62(3): 030802.